

Ultrasound Molecular Imaging of Blood Vessel Walls and Vulnerable Plaques via CXCR4-Targeted Nanoscale GVs

Chen Lin^{1,2}, Xiaoying Li¹, Yingnan Wu¹, Yuanyuan Wang³, Weijian Song¹, Fei Yan³, Litao Sun¹ 

¹Cancer Center, Department of Ultrasound Medicine, Zhejiang Provincial People's Hospital (Affiliated People's Hospital), Hangzhou Medical College, Hangzhou, Zhejiang, 310014, People's Republic of China; ²Department of Ultrasound Medicine, The First Affiliated Hospital of Wenzhou Medical University, Wenzhou, Zhejiang, 325000, People's Republic of China; ³Center for Cell and Gene Circuit Design, CAS Key Laboratory of Quantitative Engineering Biology, Shenzhen Institute of Synthetic Biology, Shenzhen Institute of Advanced Technology, Chinese Academy of Sciences, Shenzhen, 518055, People's Republic of China

Correspondence: Litao Sun; Fei Yan, Email litaosun1971@sina.com; fei.yan@siat.ac.cn

Purpose: C-X-C chemokine receptor 4 (CXCR4) mediates the inflammatory response of atherosclerotic vulnerable plaques (ASVP) and is a potential biomarker of atherosclerotic vulnerable plaques. The purpose of this study was to use the imaging ability of a new type of ultrasound contrast agent, nanoscale biosynthetic gas vesicles (GVs), on the vascular wall and to combine the specific ligand of CXCR4 to construct a targeted molecular probe to achieve early identification of atherosclerotic vulnerable plaques and guide clinical treatment decisions.

Materials and Methods: Compared three contrast agents: GVs, the micro-contrast agent SonoVue, and polyethylene glycol (PEG)-modified GVs in the carotid artery. The expression of CXCR4 in atherosclerotic plaques was demonstrated using flow cytometry and immunofluorescence experiments. Cell adhesion and in vivo ultrasound imaging experiments demonstrated their ability to target the nanoscale biosynthetic gas vesicles. The safety of GVs, PEG-GVs, and CXCR4-GVs was tested the CCK8 test, H&E staining, and serum detection.

Results: Strong CXCR4 expression was observed in plaques, whereas little expression was observed in normal vessels. GVs can produce stable contrast signals on the carotid artery walls of rats, whereas PEG-GVs can produce more lasting contrast signals on the carotid artery wall of rats. CXCR4-GVs exhibited excellent binding capability to ox-LDL-induced RAW264.7 cells. Animal experiments showed that compared with Con-GVs, CXCR4-GVs injected plaque imaging signal was stronger and more durable. In vitro scanning of vulnerable plaques in rats injected with fluorescent vesicles demonstrated that CXCR4-GVs oozed through the neovasculars within vulnerable plaques and aggregated in vulnerable plaques. Through the CCK8 test, H&E staining, and serum detection, the safety of CXCR4-GVs was confirmed.

Conclusion: CXCR4-GVs were constructed as targeted molecular probes, which can be proven to have good targeting properties to vulnerable atherosclerotic plaques.

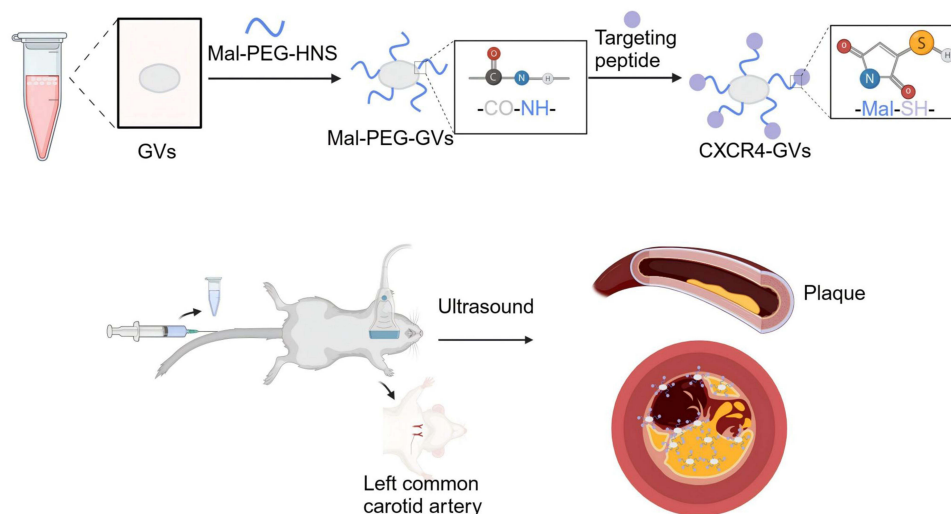
Keywords: ultrasound molecular imaging, vulnerable plaque, CXCR4, nanoscale biosynthetic gas vesicles

Introduction

Atherosclerosis Vulnerable Plaque (ASVP) is an atherosclerotic plaque with a thin fibrous cap, large necrotic core rich in lipids, internal bleeding, neovascularization, and active inflammation.¹ The insidious and unpredictable rupture of the ASVP can lead to secondary thrombosis, acute cardiovascular and cerebrovascular events, and even death.²⁻⁴ Consequently, the prompt and precise identification of ASVP proves of utmost significance in pinpointing high - risk patients, alleviating disease - related risks, and effectually governing the progression of the disease.

Ultrasound molecular imaging (UMI) uses specific molecular targets to track the biological processes of lesions and visually display the internal information of the ASVP.^{5,6} Moreover, the noninvasive nature and convenience of ultrasound technology suggest its potential as a valuable diagnostic tool.⁷ SonoVue, a microbubbles contrast agent commonly used clinically in combination with ultrasound technology to enhance imaging resolution and sensitivity, is typically between 2–5 μm in diameter, which makes them too large to extravasate and accumulate in the perivascular space.⁸⁻¹⁰ ASVP primarily conducts an analysis of

Graphical Abstract



surface ulcers by virtue of the filling defect phenomenon of the contrast agent, and the contrast signal is introduced into neovascularization for the purpose of diagnosis.¹¹ In the small plaque period, due to the overflow of angiographic signals, blood pool imaging could not identify vascular wall lesions or provide internal information of lesions, resulting in false-negative results and missed diagnoses.¹² In the previous work, our research group has successfully prepared new nanoscale biological bubbles GV from Halo, which can generate stable contrast-enhanced ultrasound signals in the blood vessel wall, and by surface modification of GV, a targeted molecular probe can be constructed for diagnosing ASVP.^{13–17} In the pathological process, 99.5% of neovascularization in the plaque originates from the outer membrane vasa vasorum.^{18,19} As the disease progresses, an increasing amount of neovascularization breaks through the media and enters the intima, providing a channel for the entry of inflammation and making the plaque vulnerable.^{20–22} Targeted nanobubbles constructed by selecting CXCR4 related to ASVP inflammation recruitment as the target are expected to enter the lesion site through neovascularization in the plaque, provide plaque information, and simultaneously display the ASVP ulcer surface, realizing multi-angle assessment of ASVP and improving diagnostic efficiency.^{23–26}

⁶⁸Ga-pentixafor, a specific CXCR4 ligand designed for positron emission tomography (PET), can precisely recognize and bind to the CXCR4 receptor, enabling the identification of macrophage infiltration in atherosclerotic plaques at the molecular level and has been widely used in clinical settings.^{27–30}

Materials and Methods

Cell Culture, Cell Model and ASVP Model

Mouse macrophage cells (RAW264.7), human umbilical vein endothelial cells (HUVEC), and mouse aortic vascular smooth muscle cells (MOVAS) were purchased from the American Type Culture Collection and cultured in DMEM high-glucose medium supplemented with 10% fetal bovine serum (FBS) and 1% penicillin-streptomycin (PS) at 37 °C and 5% CO₂. Cells were seeded in 6-well plates. To induce foam cells, HUVECs and MOVAS were given 80 µg/mL Oxidized Low-density Lipoprotein (ox-LDL) (Shenzhen Chuangxin Science and Technology Ltd., Shenzhen, China) and cultured for 72 h, RAW264.7 were given 80µg/mL ox-LDL and cultured for 48 h. Animal experiments were approved by the Ethics Committee of Shenzhen Institutes of Advanced Technology, Chinese Academy of Sciences (SIAT-IACUC-211224-HCS-YF-A2101), and were performed in strict accordance with the national standards of the People's Republic of China (Laboratory animal: Guideline for ethical review of animal welfare [GB/T 35892–2018]). Male Sprague-Dawley rat (SD rat) (8 weeks old, body weight 200 ± 20 g) were supplied by Zhanyan Biotechnology Co., Ltd., Shanghai. The rats were kept in an SPF room on a 12/12 hour light–dark

cycle with freely available food and water. An accelerated atherosclerotic rat model was induced by a combination of a high-fat, high-cholesterol diet (cholesterol 1%, fat 10%, yolk powder 3%) and 2F Fogarty balloon catheter endothelial injury. Atherosclerosis was initiated after one week of a high-fat, high-cholesterol diet. Anesthesia was maintained with isoflurane inhalation. The left carotid arteries were injured with a 2.0 Fogarty balloon catheter, as described earlier. Briefly, a balloon catheter was gently advanced through the external carotid artery into the left common carotid artery. The balloon was gently inflated to 2 atm and then retracted. This procedure was repeated thrice for each rat. The balloon catheter was removed, the incision closed with sutures, and the rats were allowed to recover. Plaques in these rats were observed and monitored using weekly ultrasound.

Preparation of GVs, PEG-GVs, Con-GVs, and CXCR4-GVs

Halo bacteria were cultured in ACTT culture medium (250 g NaCl, 20 g MgSO₄, 3 g Trisodium citrate, 2 g KCl, 3 g Yeast extract, 5 g Tryptone, 1 L purified water) at 37 °C continuously for 7–9 days at 220 rpm/min, these cultured bacteria were transferred to the separatory funnel for 1–2 weeks to collect floated bacteria. Floating bacteria were lysed using TMC lysate buffer (10 mm Tris-HCl, 2.5 mm MgCl₂, 2 mm CaCl₂, pH 7.5), and GVs were centrifuged at 300×g at 4 °C. The isolated GVs were washed with phosphate buffered saline (PBS), purified three times by centrifugation at 250 g for 3 h, and finally stored in PBS at 4 °C. GV concentration was estimated using a full-wavelength microplate reader (Scientific Multiskan GO Thermo Fisher, Waltham, MA, USA) at an OD₅₀₀.

In the presence of 1-ethyl-(3—dimethyl aminopropyl) carbamide (EDC) and N-hydroxysuccinimide (NHS), PEG was coupled to the GVs surface through an amidation reaction. EDC (4 mg) and NHS (6 mg) were dissolved in GVs solution and activated at room temperature for 2–4 h. Subsequently, the activated GVs were slowly added to a methoxypolyethylene glycol amine (PEG-amine, molecular weight = 5 kDa) (523 mg) solution and incubated at 4 °C overnight to ensure full combination of PEG-amine and GVs. The obtained solution was centrifuged and rinsed with PBS 3–4 times to remove excess EDC, NHS, and PEG-amine.

The GVs were coupled to alpha-maleimide-omega-N-hydroxysuccinimide ester polyethylene glycol (Mal-PEG-NHS, molecular weight = 2 kDa) through an amidation reaction, and the targeted peptides (2-Nal-Gly-Tyr-N-me-Orn(Cys)-Arg³¹) or the control peptide sequence, 2-Nal-N-me-Gly-Arg-Orn(Cys)-Tyr, were linked to Mal-PEG-GVs through a thioether reaction. Briefly, Mal-PEG-NHS (40 mg) was dissolved in 1 mL GVs (OD₅₀₀:3.5) and incubated at 4 °C for 2–4 h, then centrifuged and rinsed with PBS 3–4 times to remove unbound Mal-PEG-NHS. Next, a PBS solution containing 1 mg of the targeted peptides was added to the Mal-PEG-GVs and incubated at 4 °C overnight. The reaction mixture was centrifuged and rinsed with PBS 3–4 times. FITC-labeled CXCR4-GVs were obtained by adding AF488-NHS (Beyotime Biotechnology, Shanghai, China). Similar rinse steps were used to remove free AF488.

Flow Cytometry and Immunofluorescence Staining

For flow cytometry analysis, 1×10⁶ in vitro cultured ox-LDL-induced RAW264.7 cells were directly stained with anti-CXCR4 antibody for 1 h at 4 °C and Alexa Fluor 488-conjugated secondary antibody for 45 min at room temperature, followed by analysis with flow cytometry (BD FACSAria™III, BD, Franklin Lakes, USA). The RAW264.7 cells were not induced by ox-LDL using the same antibody, and a secondary antibody was used as the control. HUVEC and MOVAS were treated in the same manner.

Plaque and normal blood vessel tissues from rats were collected after euthanasia according to the IACUC and embedded in OCT. Frozen sections were made a microtome cryostat (Leica CM1950, Germany) (thickness = 8 μm). The tissue sections were blocked with 3% BSA for 30 min and stained with an anti-CXCR4 antibody overnight at 4 °C. The sections were then incubated with an Alexa Fluor 488-conjugated secondary antibody (Beyotime Biotechnology, Shanghai, China) for 1 h at room temperature. 4'6-diamidino-2-phenylindole (DAPI) was used for staining nuclei. Fluorescence images were acquired using an inverted microscope (IX73, Olympus).

The Characterization and in vitro Imaging of CXCR4-GVs

The GVs solution was diluted, placed on a copper net, negatively stained with 2% phosphotungstic acid, and dried at room temperature. GVs morphology were examined using transmission electron microscopy (TEM) (Hitachi H-7650,

Hitachi Limited, Tokyo, Japan). The absorbance peaks of CXCR4-GVs and Con-GVs were detected using a Fourier infrared spectrometer (FT-IR, Bruker, Germany). The particle size and potential of GVs, PEG-GVs, Mal-PEG-GVs, and CXCR4-GVs were measured using a Zetasizer analyzer (Zetasizer Nano S90, Malvern, Worcestershire, UK).

Targeting Ability Testing of CXCR4-GVs

RAW264.7 cells were cultured overnight in a 24-well plate (5×10^4 cells/well), and RAW264.7-derived foam cells were induced using the above method after the cells were attached to the wall. After washing three times with PBS, FITC-labeled CXCR4-GVs or Con-GVs were added to the walls, and the cells were incubated darkly for 5–6 min. Free CXCR4-GVs or Con-GVs were rinsed with PBS 3–5 times, after which the cells were fixed with 4% paraformaldehyde for 15 min and stained with DAPI. The adhesion of CXCR4-GVs or Con-GVs to the cells was observed by random field selection under an inverted microscope. Simultaneously, a competitive binding inhibition experimental group was established (the cells were pre-incubated with excess free targeting peptides at room temperature for 30 min to occupy the CXCR4 receptor on the cell surface, and FITC-labeled CXCR4-GVs was added to observe cell adhesion to the cells).

Vascular Wall Imaging Capabilities of GVs

Healthy rats were randomly injected with SonoVue (300 μ L, 45 μ g/mL), GVs (300 μ L, OD₅₀₀ = 3.5), or PEG-GVs (300 μ L, OD₅₀₀ = 3.5) via the tail vein. Ultrasound imaging was performed using a 3.0–11.0 MHz line array transducer equipped with ultrasound diagnostic equipment (Mindray Resona 7, Mindray, Shenzhen, China). After this number completely disappeared, the next injection was performed at intervals of more than half an hour, and all parameters (acoustic power, 5.13%; mechanical index, 0.167; contrast gain, 65 dB) remained unchanged during imaging.

In vivo Ultrasound Molecular Imaging of CXCR4-GVs

During imaging, rats ($n = 6$) were anesthetized with 2% isoflurane and warmed using a heating pad. Model rats were randomly injected with Con-GVs (300 μ L OD₅₀₀ = 3.5) or CXCR4-GVs (300 μ L OD₅₀₀ = 3.5) via the tail vein. Ultrasound imaging was performed using a 3.0–11.0 MHz line array transducer equipped with a Mindray Resona 7. After the signals completely disappeared, the next injection was performed at 30 min intervals, and all parameters (acoustic power, 5.13%; mechanical index, 0.167; contrast gain, 65 dB) remained unchanged during imaging.

Histological Examination

To confirm that GVs were able to pass through the endothelial gaps of plaques, ASVP rats ($n = 6$) were injected with 300 μ L FITC-labeled Con-GVs or FITC-labeled CXCR4-GVs via the caudal vein, and plaques were collected after 10 min and used as frozen sections. Tumor sections were fixed with 4% PFA and stained with DAPI for nuclei and anti-CD31 antibody (Abcam, Cambridge, UK) for plaque vessels. Cy5-conjugated goat anti-rabbit secondary antibody (Abcam, Cambridge, UK) was used to visualize vessels.

Biosafety Testing of CXCR4-GVs

The Cell Counting Kit-8 (CCK-8) (Beyotime Biotechnology, Shanghai, China) was used to determine cell viability. Briefly, RAW264.7 cells were cultured in 96-well cell plates (5×10^4 cells per well) and exposed to 100 μ L GVs, PEG-GVs, or CXCR4-GVs (OD₅₀₀ = 2.0, 2.5, 3.0, or 3.5). CCK-8 solution was then added to the plates and incubated for 12 h. The absorbance was measured at a wavelength of 450 nm.

Twelve rats were systemically administered PBS, GVs, PEG-GVs, or CXCR4-GVs (300 μ L, OD₅₀₀ = 3.5). Blood samples were collected from the ophthalmic arteries after 1 and 7 days to detect liver function markers (alanine aminotransferase [ALT], aspartate aminotransferase [AST]) and kidney function markers (blood urea nitrogen, BUN, creatinine, and CREA). After blood collection, the mice were sacrificed immediately and the main organs, including the heart, liver, spleen, lungs, and kidneys, were acquired and fixed with paraformaldehyde (4%, w/v) for H&E staining.

Statistical Analysis

Quantitative data on the vascular wall imaging capability of the GVs are expressed as the mean \pm SD. GraphPad Prism software (version 6.0) was used for plotting graphs and data analysis. Differences between two groups were compared using an independent sample *t*-test. $P < 0.05$.

Results

Characterization of GVs, PEG-GVs and CXCR4-GVs

TEM examination clearly showed that the GVs were monodisperse, with a rugby-ball-shaped structure (Figure 1A). In contrast to the GVs and Mal-PEG-GVs, CXCR4-GVs and Con-GVs were observed the absorbance peaks at 2327.33 cm^{-1}

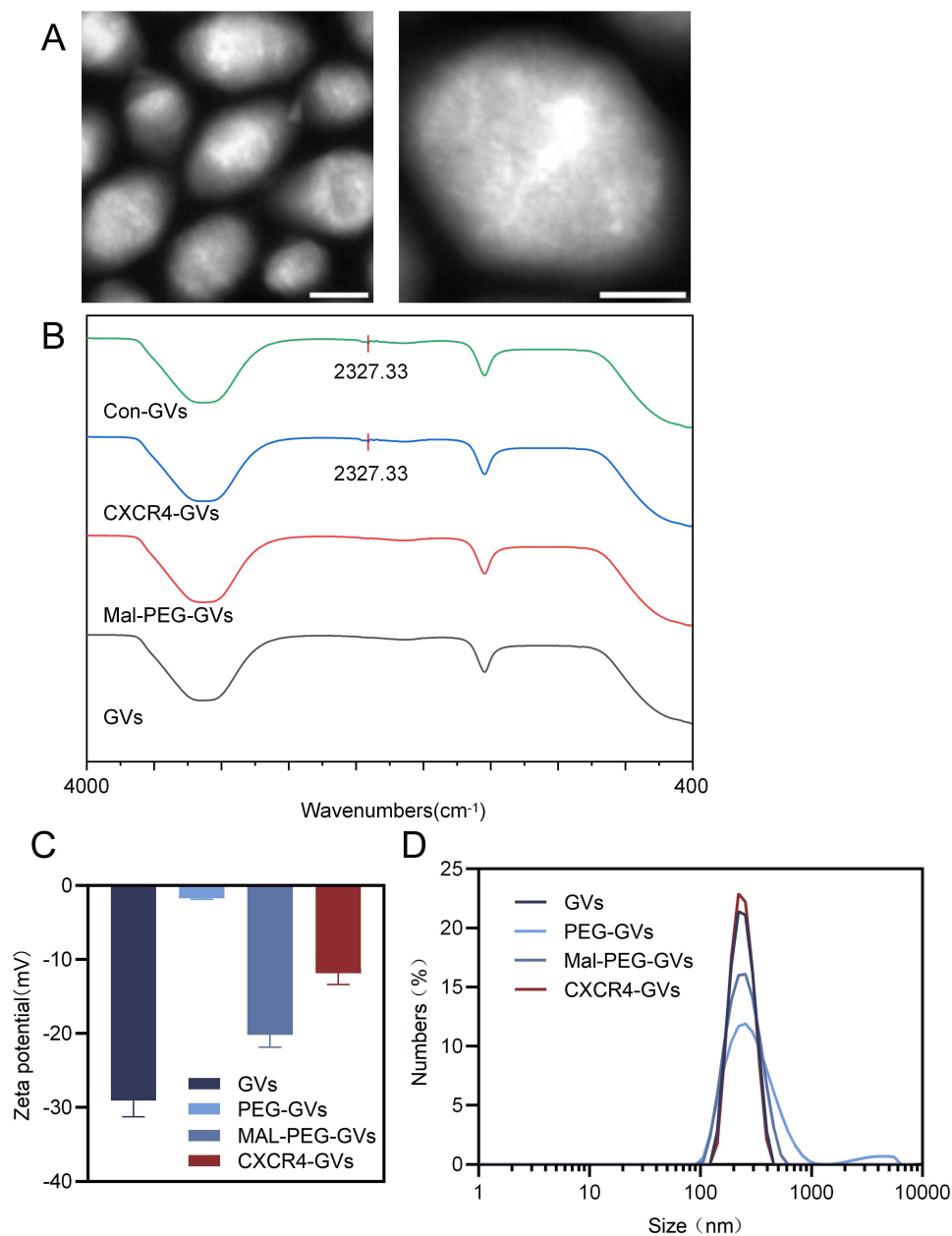


Figure 1 Preparation and characterization of GVs, PEG-GVs, and CXCR4-GVs. **(A)** TEM images of isolated GVs (left and right). The scale bars are 100 nm (left), 50 nm (right), respectively; **(B)** infra-red spectrogram of GVs, Mal-PEG-GVs, Con-GVs and CXCR4-GVs; **(C)** Zeta potential of GVs, PEG-GVs, Mal-PEG-GVs and CXCR4-GVs; **(D)** Size distribution of GVs, PEG-GVs, Mal-PEG-GVs and CXCR4-GVs; Data of **(C)** and **(D)** represent the mean \pm SD from 3 independent experiments.

(Figure 1B). The zeta potential of GVs, PEG-GVs, Mal-PEG-GVs and CXCR4-GVs were -29.10 ± 2.14 mV, -1.70 ± 0.14 mV, -20.20 ± 1.65 mV and -11.83 ± 1.55 , respectively (Figure 1C). The average particle hydrodynamic diameters were 217.45 ± 4.65 nm for GVs, 272.65 ± 8.95 nm for PEG-GVs, 243.50 ± 3.50 nm for Mal-PEG-GVs and 265.25 ± 3.05 nm for CXCR4-GVs, respectively (Figure 1D).

CXCR4 Expression in Cell and Tissue

The expression of CXCR4 in RAW264.7, HUVEC, and MOVAS-derived foam cells was detected using flow cytometry. The CXCR4-positive rate on the surface of RAW264.7-derived foam cells, HUVEC-derived foam cells, and MOVAS-derived foam cells were 64.9%, 0.14%, and 2.42%, respectively (Figure 2A). CXCR4 expression in plaque and normal carotid tissues was also evaluated. From Figure 2B and C, we can see a strong green fluorescence signal in plaque tissue, whereas almost no green fluorescence signals were observed in normal carotid tissue.

Binding of CXCR4-GVs to RAW264.7-Derived Foam Cells

To determine the ability of CXCR4-GVs to bind to CXCR4 receptors on the cell surface, cultured RAW264.7-derived foam cells were incubated with CXCR4-GVs or Con-GVs ($OD_{500} = 2.0$). We could see that after 5 min incubation, the binding ability of FITC-labeled CXCR4-GVs to RAW264.7-Derived Foam Cells was significantly higher than that of FITC-labeled Con-GVs (Figure 3A). The ability of CXCR4-GVs to bind to RAW264.7-foam cells decreased because of the pre-blocking of excessively targeted peptides. Quantitative analysis showed that the average fluorescence intensity of Con-GVs, CXCR4-GVs and blocking groups was $29.92 \text{ a.u.} \pm 1.80 \text{ a.u.}$, $99.97 \text{ a.u.} \pm 21.46 \text{ a.u.}$ and $38.19 \text{ a.u.} \pm 4.74 \text{ a.u.}$, respectively (Figure 3B).

In vitro Imaging of CXCR4-GVs

To evaluate the contrast imaging performance of CXCR4-GVs, different concentrations of CXCR4-GVs from OD_{500} 0.5 to 2.0 were imaged in contrast mode. Figure 4A clearly shows that GVs, Con-GVs, and CXCR4-GVs exhibit significantly enhanced contrast signals. The higher the GVs, Con-GVs and CXCR4-GVs concentrations, the stronger the contrast signals of GVs, Con-GVs, and CXCR4-GVs. Quantitative analysis of average signal intensity revealed that GVs, Con-GVs, and CXCR4-GVs had comparable contrast signals at the same concentration (Figure 4B).

Vascular Wall Imaging Capability of GVs

In this study, SonoVue, GVs, and PEG-GVs were injected intravenously into rats at intervals of > 30 min to compare their imaging abilities in blood vessels. Angiography was performed in CEUS mode. As shown in Figure 5A, GVs generated stable angiographic signals on the carotid artery wall of rats, and SonoVue only imaged the carotid blood pool of rats. Notably, PEG-GVs could obtain longer-lasting angiographic signals in the carotid artery walls of rats.

SonoVue, GVs, and PEG-GVs were injected into SD rats in a plaque model for in vivo imaging, and it was found (Figure 5B) that SonoVue could be used for vascular lumen imaging. Owing to the overflow of imaging signals, we could not observe any difference in the imaging signals between the plaque in the anterior wall of the carotid artery and the lumen. By contrast, GVs can generate angiographic signals from the blood vessel wall and accurately outline the shape of the plaque located in the anterior wall of the carotid artery. After injection of PEG-GVs, the contrast signal and cycle time in the vascular wall and plaque were stronger than those of the GVs.

In vivo UMI

Next, we evaluated the targeting ability of CXCR4-GVs in plaque rats with plaques. The results (Figure 6A) showed no contrast signals in the intravascular plaque prior to injection of CXCR4-GVs or Con-GVs. As shown in Figure 6B, there was no significant difference in the peak signal intensities between the Con-GVs (190.80 ± 8.22) and CXCR4-GVs (207.30 ± 4.43) in the plaque. However, the signal intensity in the plaques of the CXCR4-GVs was significantly higher than that of the Con-GVs after 0.5 min (Figure 6C). The quantitative analysis of signal intensity in the plaque received with CXCR4-GVs achieved 14.91-fold higher than those of Con-GVs at 5 min (69.19 ± 4.64 vs 7.52 ± 10.53 , $P < 0.001$), 11.94-fold higher than those of Con-GVs at 10 min (34.52 ± 14.76 vs 2.89 ± 3.47 , $P < 0.05$), respectively.

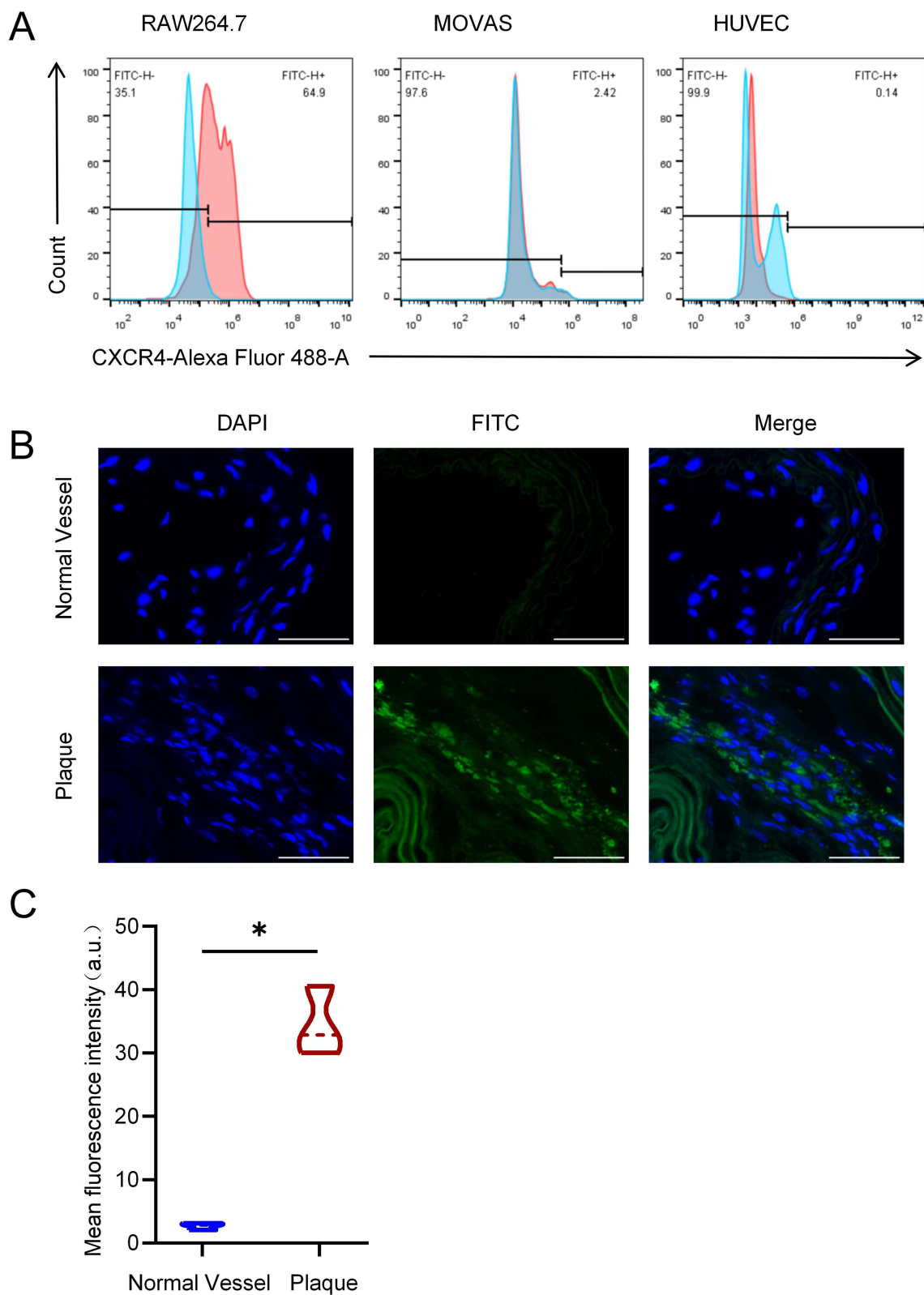


Figure 2 CXCR4 expression in foam cells and plaque tissues. **(A)** Flow cytometry analysis for the foam cell surface expression level of CXCR4 protein on RAW264.7 cells, MOVAS cells and HUVEC cells. Scale bars are 50 nm; **(B)** Immunofluorescence Staining in normal vessels and plaque tissues; **(C)** Quantification analysis of mean fluorescence intensity from **(B)**. * $p < 0.05$.

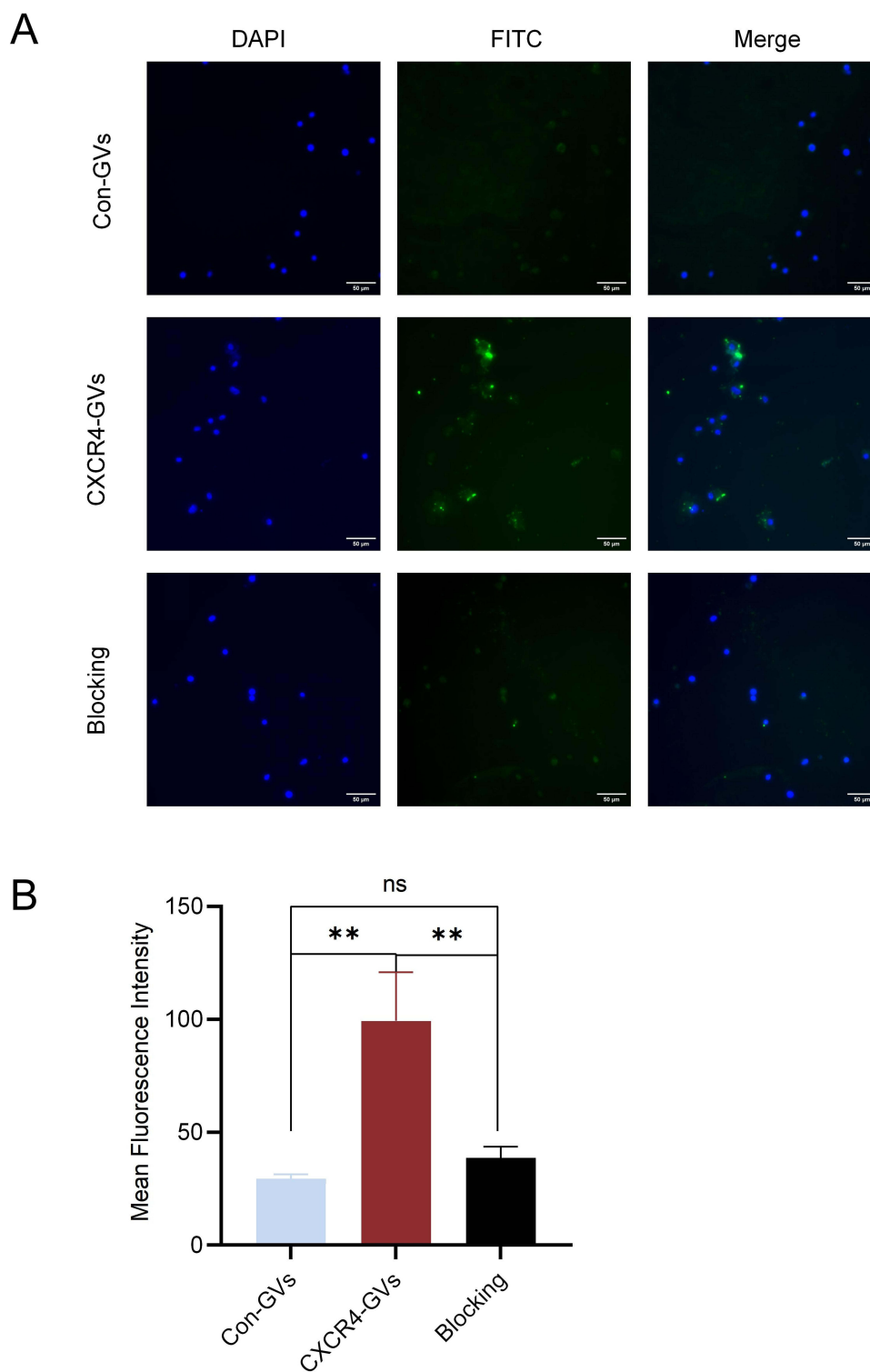


Figure 3 In vitro binding of CXCR4-GVs to RAW264.7-derived foam cells. **(A)** Representative fluorescent microscope images of RAW264.7-derived foam cells incubated with FITC-labeled Con-GVs, FITC-labeled CXCR4-GVs and free targeting peptide + FITC-labeled CXCR4-GVs. Green represents FITC-labeled GV and blue represents cell nuclei stained with DAPI. Scale bar: 50 μ m. **(B)** Quantification of fluorescence intensity from **(A)**. The data in **(B)** represent the mean \pm SD of three independent experiments. ** $p < 0.01$, ns no significance.

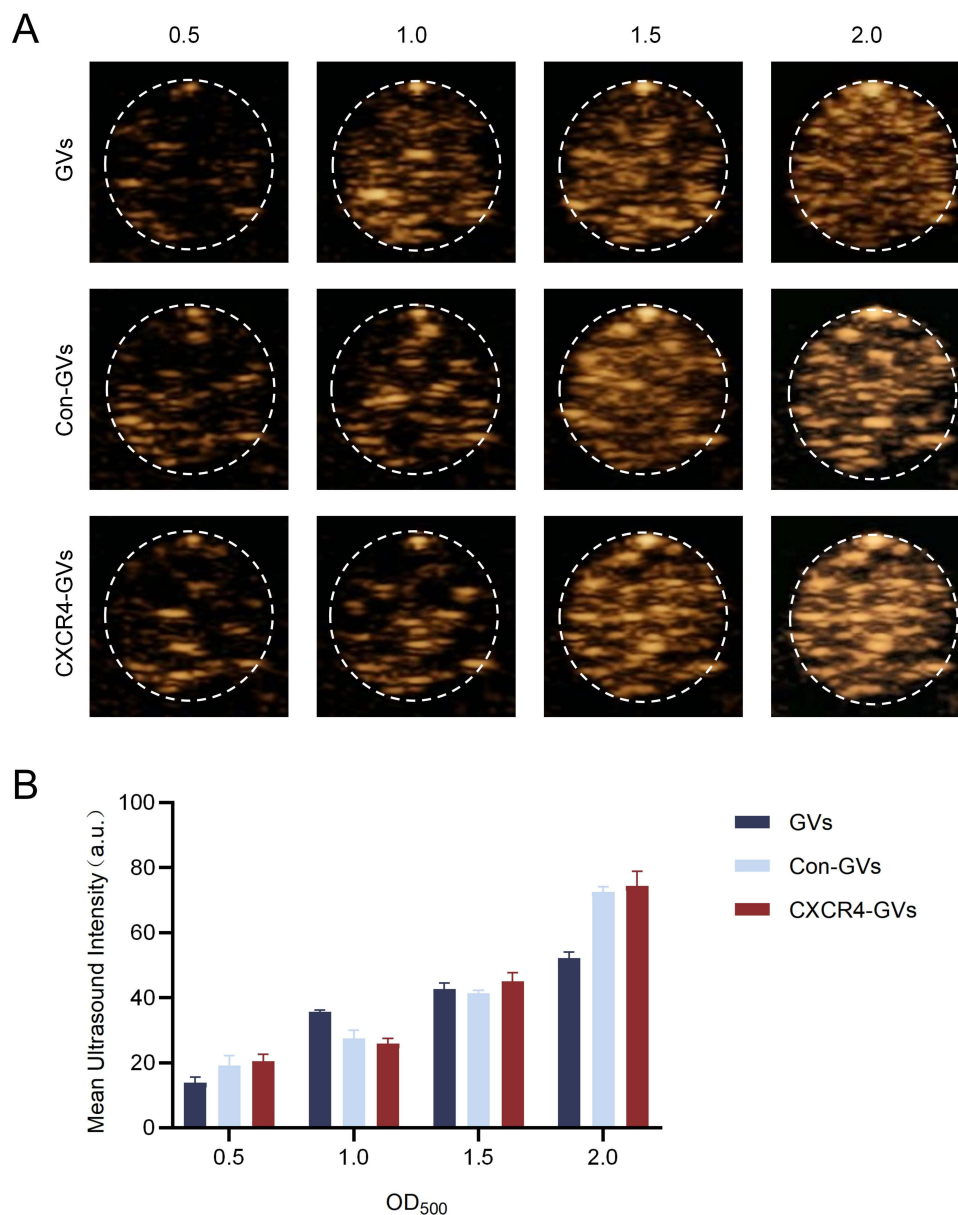


Figure 4 In vitro ultrasound contrast imaging of GV, con-GV, and CXCR4-GV. **(A)** Ultrasound contrast images of GV, Con-GV, and CXCR4-GV at different concentrations ($OD_{500} = 0.5-2.0$). **(B)** Quantification of the mean ultrasound signal intensities from **(A)**. Data represent the mean \pm SD of three independent experiments.

Distribution of CXCR4-GVs

To further verify the distribution of CXCR4-GVs in rat plaques, FITC-labeled CXCR4-GVs or Con-GVs were injected into rats via the caudal vein and the sections were sacrificed after 10 min. From the [Figure 7A](#), it can be observed that numerous FITC-labeled CXCR4-GVs were not only present in the vascular system, but also in the extravascular space of the plaque, indicating that CXCR4-GVs is leaking from the neovasculature within the plaque. Three fields were randomly selected for quantitative fluorescence intensity analysis ([Figure 7B](#)), and the fluorescence signal of the CXCR4-GVs was significantly stronger than that of the Con-GVs ($P < 0.001$).

In vitro and in vivo Biosafety of GV, PEG-GV and CXCR4-GVs

The results of the in vitro cytotoxicity assay were assessed by incubating different concentrations of GV, PEG-GV and CXCR4-GVs with MB49 cells, followed by viability assay using the CCK-8 kit. [Supplementary Figure 1](#) clearly shows that

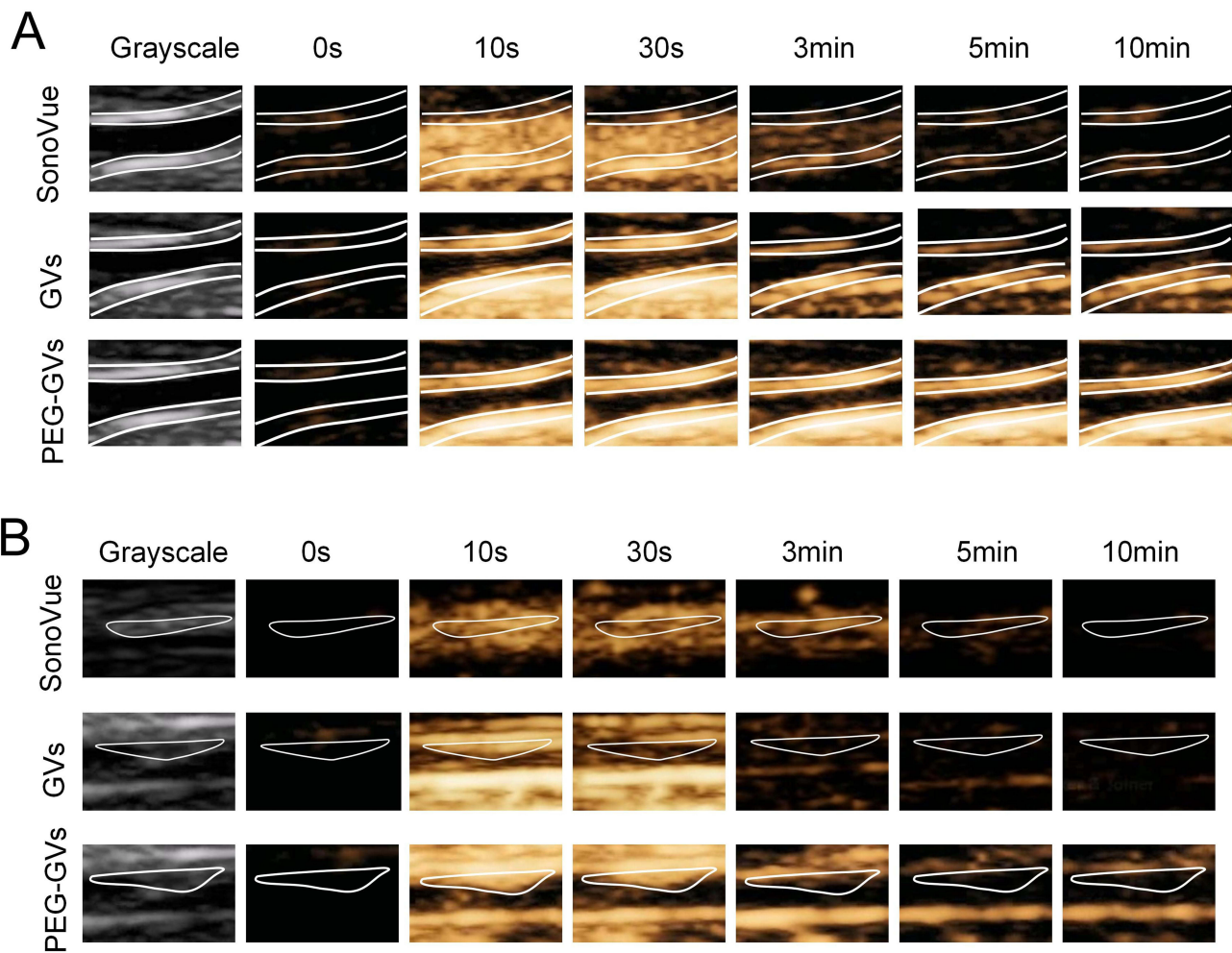


Figure 5 Vascular wall imaging capabilities of GVs. **(A)** Contrast-enhanced images of SonVue, GVs, and PEG-GVs after intravenous injection into the normal carotid artery. **(B)** Contrast-enhanced images of SonVue, GVs, and PEG-GVs after intravenous injection into the plaque carotid artery.

no obvious cytotoxicity to RAW264.7 cells was found at all tested concentrations (OD500 = 2.0, 2.5, 3.0, and 3.5). H&E staining showed no pathological damage to the heart, liver, spleen, lungs, and kidneys after injection of GVs, PEG-GVs, and CXCR4-GVs compared with the PBS control (Figure 8A–D). Hematologic data of GVs, PEG-GVs, and CXCR4-GVs injected intravenously into healthy C57BL/6 mice on the first day and on the seventh day were also analyzed, revealing that the indices of (alanine aminotransferase (ALT), aspartate aminotransferase (AST), and renal function (alkaline phosphatase, ALP; Blood urea nitrogen, BUN; Serum creatinine, CREA) were still within the normal range (Figure 8E).

Discussion

The precise identification of ASVP assumes a pivotal role in determining the progression of the disease and its prognosis. In the present study, we engineered an innovative, targeted molecular probe, namely CXCR4 - GVs, specifically designed for the diagnosis of ASVP. Our results showed that the targeting of CXCR4-GVs can be visualized in contrast-enhanced ultrasound mode and has good sensitivity for identifying ASVP. Successful identification of ASVP may contribute to several aspects. First, because of their small particle size, GVs have inherent characteristics in vascular wall imaging, especially in vascular wall lesions; second, the targeting peptide, 2-Nal-Gly-Tyr-N-me-Orn(Cys)-Arg from 68Ga-pentixafor, designed as a specific CXCR4 ligand for positron emission tomography (PET), is able to precisely recognize and bind to the CXCR4 receptor. As shown in Figure 5, our study substantiated the efficacy of gas-filled GVs for imaging vascular wall lesions by conducting in vivo ultrasound imaging experiments on the carotid artery, confirming that GVs

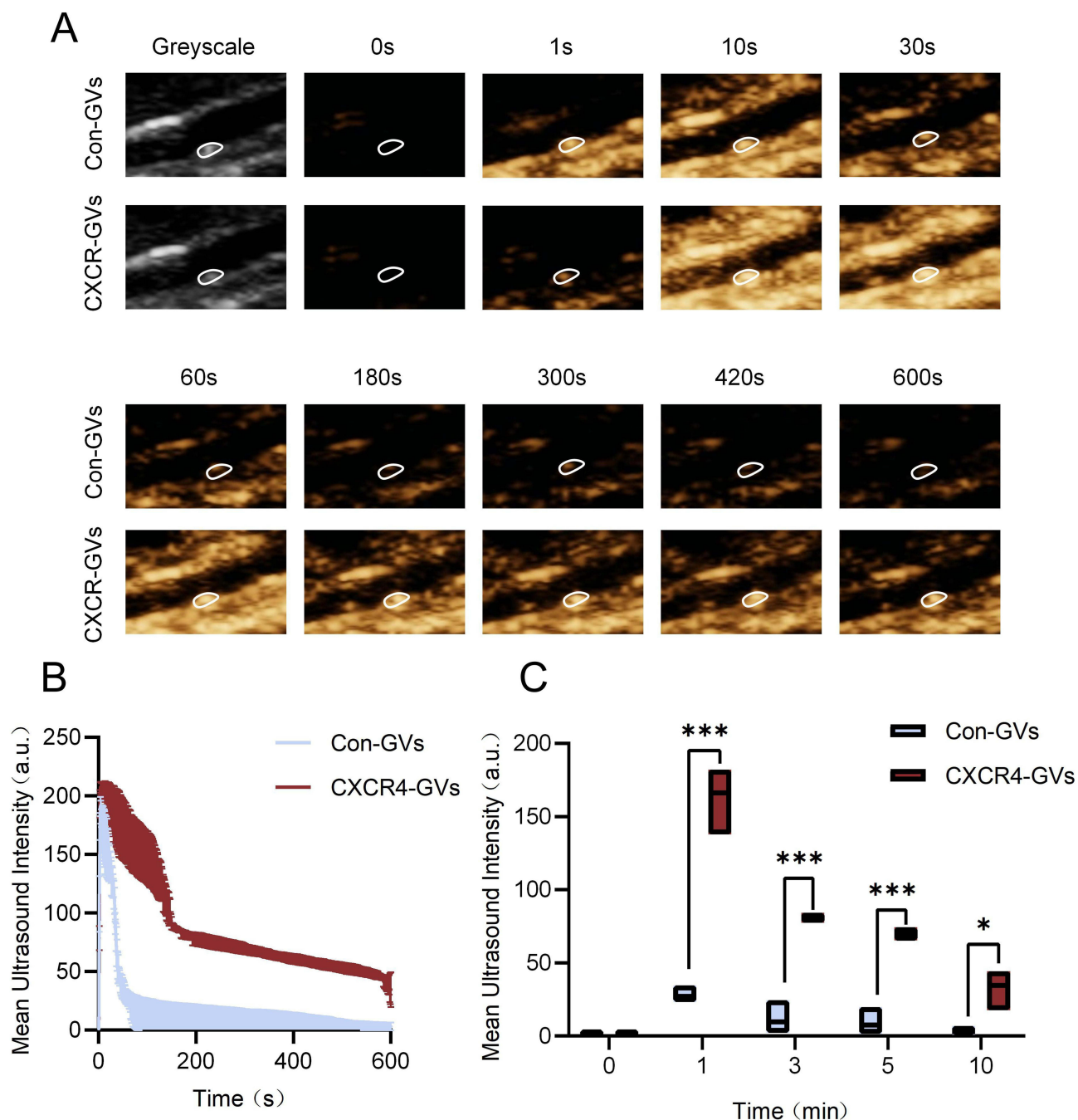


Figure 6 In vivo ultrasound molecular imaging of plaques. **(A)** Non-linear contrast images of Con-GVs and CXCR4-GVs ($OD_{500} = 3.5$) at different time points after intravenous injection. **(B)** Time-intensity curves of Con-GVs and CXCR4-GVs after intravenous injection. **(C)** Contrast signal intensities of tumors treated with Con-GVs and CXCR4-GVs at 1, 3, 5, and 10 minutes. Data **(B and C)** represent the mean \pm SD of three independent experiments. * $p < 0.05$, *** $p < 0.001$.

outperformed SonoVue in diagnosing vascular wall lesions. Furthermore, the data indicated that surface modification of nanoparticles with polyethylene glycol (PEG) effectively mitigates Reticuloendothelial System (RES) uptake and prolongs blood circulation time, thereby improving imaging outcomes.³² We further opted for the vascular wall imaging capabilities of GVVs by conjugating them with PEG for their application in vascular wall imaging. This modification was intended to mitigate the immunogenicity associated with protein-shelled GVVs and to minimize non-specific binding and clearance within the body, thereby improving imaging efficacy at vascular wall lesion sites.

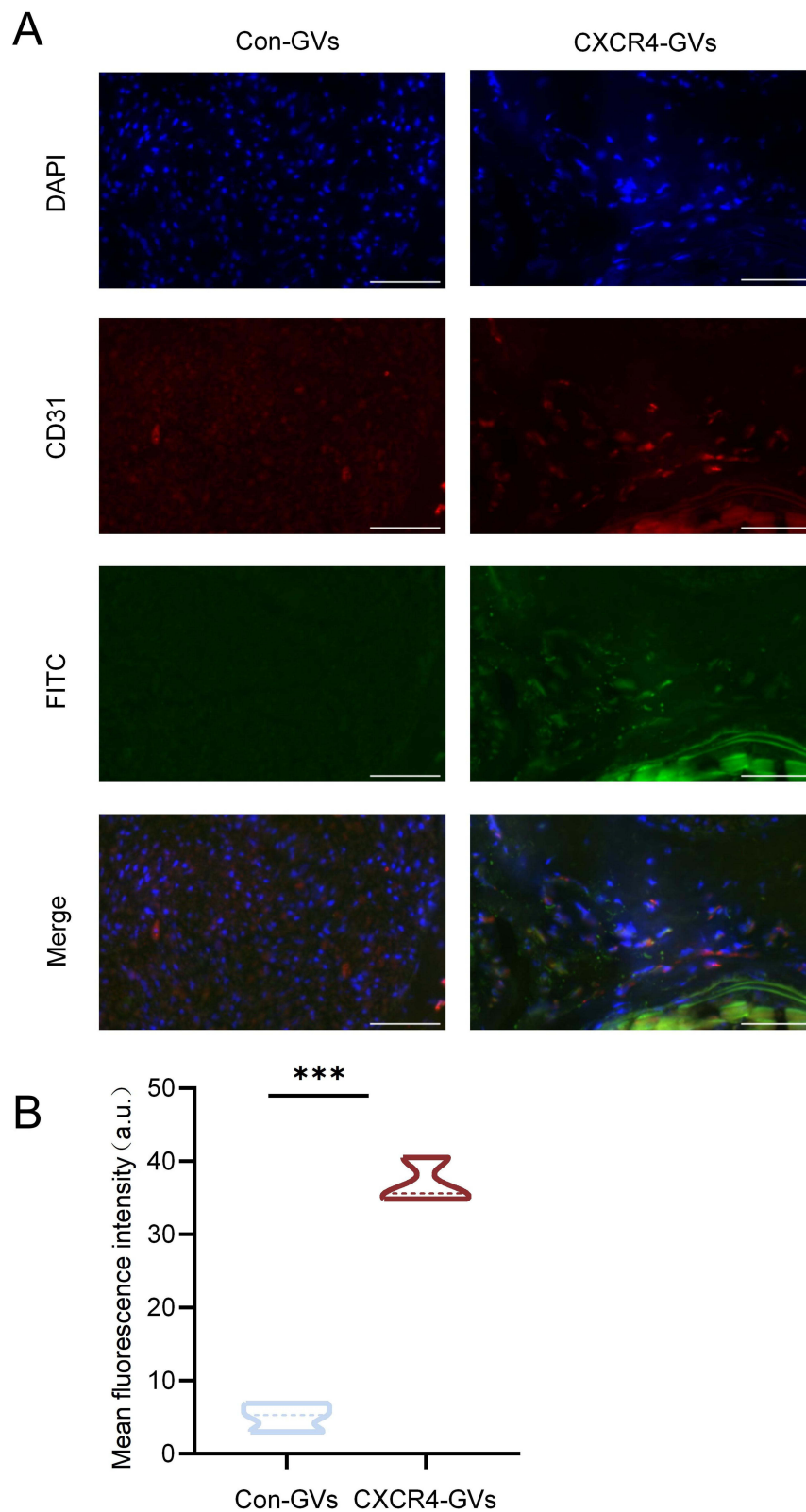


Figure 7 Histological analysis. **(A)** Representative fluorescence images of plaque sections from rats injected with FITC-labeled Con-GVs or FITC-labeled CXCR4-GVs. Green indicates GVs, red indicates anti-CD31 antibodies, and blue indicates cell nuclei stained with DAPI. Scale bar: 50 μ m. **(B)** Mean fluorescence intensity of plaque sections in three random view fields. Data represent the mean \pm SD of three independent experiments. *** $p < 0.001$.

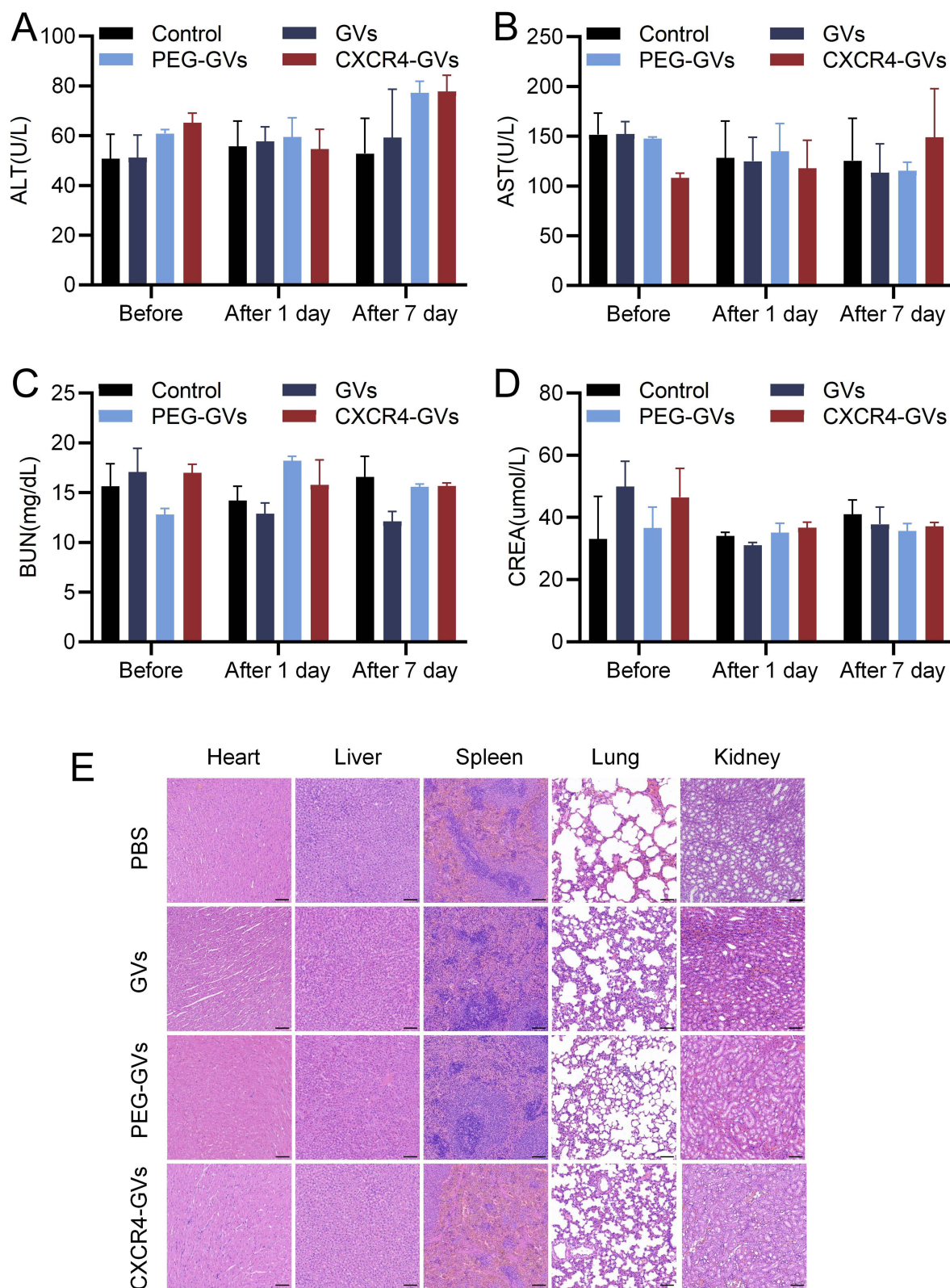


Figure 8 Biosafety analysis. (A–D) Liver and kidney function indices of rats treated with the same volume of PBS, PEG-GV, and CXCR4-GVs. The units of ALT, AST, and ALP were U/L, and those of BUN and CREA were $\mu\text{mol/L}$. (E) Representative H&E sections of the main organs (heart, liver, spleen, lung, and kidney) from mice treated with PBS, GV, PEG-GVs, or CXCR4-GVs for seven days. Scale bars: 100 μm . Data represent the mean \pm SD of three independent experiments.

To achieve molecular-targeting function of GVs and extend their circulation time, we fabricated the targeted molecular probe CXCR4-GVs through a two-step modification strategy. The first step was to link MAL-PEG-NHS with GVs, with one end of the molecule reacting with the protein shell of the GVs and the other end retaining the Mal group, providing an active site for subsequent connections. Next, the medial end of MAL-PEG-NHS connects with the thiol group of the modified peptide, forming a “bridge” to transform GVs into CXCR4-GVs with targeting functionality. We compared the imaging of Con-GVs and CXCR4-GVs in vitro and found that the contrast signals of both Con-GVs and CXCR4-GVs increased with increasing concentration of GVs. The contrast signals of Con-GVs and CXCR4-GVs were similar at the same GV concentration. This indicates that the modified GVs still had good imaging capabilities. As shown in Figure 6, in vivo animal experiments demonstrated that CXCR4-GVs produced stronger signals in the plaque tissue. In conclusion, we combined a new contrast agent capable of imaging the vessel wall to achieve early and accurate identification of ASVP, which may shorten the time required for clinical translation.

Neovascularization in ASVP is an important channel for transporting inflammatory mediators, regulating plaque metabolism, and affecting plaque progression owing to its high permeability.³² At the same time, plaque neovascularization promoted the growth of outer membrane microvessels at the site of wall rupture, resulting in the formation of immature vascular networks, and thus making vulnerable plaques fragile and highly permeable.^{33,34} The translocation of nanoparticles into the atherosclerotic endothelium relies on microvascular permeability.³⁵ Owing to neovascularization within vulnerable plaques, they also exhibit a tumor-like EPR effect, allowing small nanoparticles to penetrate the vascular wall and accumulate within the vulnerable plaques.^{36–39} Phagocytosis within atherosclerotic lesions and the EPR-like effect provide a passive mechanism for CXCR4-GVs to enter plaques, thus enabling the identification of vulnerable plaques. Meanwhile, the surface ligands of CXCR4-GVs provided an active role in binding with plaques, resulting in better targeting imaging of CXCR4-GVs relative to Con-GVs.

In the future, by using this molecular - targeted probe to load drugs, we can achieve the integration of diagnosis and treatment. Additionally, the real - time detection of drug release during the treatment process can be realized, which is expected to provide new strategies for the prevention and treatment of clinical cardiovascular and cerebrovascular events.^{40,41}

Conclusion

In summary, we used biosynthetic GVs to develop a molecular probe, CXCR4-GVs, with imaging and targeting properties. We discovered a unique vascular wall imaging technique. For the first time, we developed a novel targeted molecular probe, CXCR4-GVs, which provides a new method for early diagnosis of atherosclerotic vulnerable plaques and for future clinical translation.

Acknowledgment

This study was supported by the National Key R&D Program of China (2020YFA0908800), National Natural Science Foundation of China (82071929, 82202158, and 32171365), Guangdong Innovation Platform of Translational Research for Cerebrovascular Diseases, and Shenzhen Medical Research Fund (Grant No. D2301012).

Disclosure

The authors declare that they have no known competing financial interests or personal relationships that could influence the work reported in this study.

References

1. Piepoli MF, Hoes AW, Hoes AW; Authors/Task Force Members, et al. 2016 European guidelines on cardiovascular disease prevention in clinical practice: the sixth joint task force of the European society of cardiology and other societies on cardiovascular disease prevention in clinical practice (constituted by representatives of 10 societies and by invited experts) developed with the special contribution of the European Association for Cardiovascular Prevention & Rehabilitation (EACPR). *Atherosclerosis*. 2016;252:207–274. doi:10.1016/j.atherosclerosis.2016.05.037
2. GBD 2013 Mortality and Causes of Death Collaborators. Global, regional, and national age-and sex-specific all-cause and cause-specific mortality for 240 causes of death, 1990–2013: a systematic analysis for the global burden of disease study 2013. *Lancet*. 2015;385(9963):117–171.
3. Libby P, Buring JE, Badimon L, et al. Atherosclerosis. *Nat Rev Dis Primers*. 2019;5(1):56.
4. Petkovic A, Erceg S, Munjas J, et al. LncRNAs as regulators of atherosclerotic plaque stability. *Cells*. 2023;12(14):1832. doi:10.3390/cells12141832

5. Ozawa K, Lindner JR. Ultrasound molecular imaging: insights into cardiovascular pathology. *J Echocardiogr.* 2020;18(2):86–93. doi:10.1007/s12574-020-00463-z
6. Bäck M, Yurdagul A Jr, Tabas I, Öörni K, Kovanen PT. Inflammation and its resolution in atherosclerosis: mediators and therapeutic opportunities. *Nat Rev Cardiol.* 2019;16(7):389–406. doi:10.1038/s41569-019-0169-2
7. Yu M, Zhou C, Liu L, et al. Interactions of renal-clearable AuNPs with tumor microenvironments: vasculature and acidity effects. *Angew Chem Int Ed Engl.* 2017;56(15):4314–4319. doi:10.1002/anie.201612647
8. Endo-Takahashi Y, Negishi Y. Microbubbles and nanobubbles with ultrasound for systemic gene delivery. *Nat.Pharmaceutics.* 2020;12(10):964. doi:10.3390/pharmaceutics12100964
9. Finn AV, Jain RK. Coronary plaque neovascularization and hemorrhage: a potential target for plaque stabilization. *JACC Cardiovasc Imaging.* 2010;3(1):41–44. doi:10.1016/j.jcmg.2009.11.001
10. Sans M, Panés J, Ardite E, et al. VCAM-1 and ICAM-1 mediate leukocyte-endothelial cell adhesion in rats with experimental colitis. *Gastroenterology.* 1999;116(4):874–883. doi:10.1016/S0016-5085(99)70070-3
11. van den Oord SC, ten Kate GL, Akkus Z, et al. Assessment of subclinical atherosclerosis using contrast-enhanced ultrasound. *Eur Heart J Cardiovasc Imaging.* 2013;14(1):56–61. doi:10.1093/ehjci/jes109
12. Wang C, Yang S, Chen X, He Q, Zhao K, Hu J. Molecular imaging diagnosis of atherosclerotic vulnerable plaque in rabbit carotid artery using a self-assembled nanoscale ultrasound microbubble contrast agent. *Rev Cardiovasc Med.* 2021;22(4):1657–1666. doi:10.31083/j.rcm2204173
13. Wei M, Lai M, Zhang J, Pei X, Yan F. Biosynthetic gas vesicles from *Halobacterium NRC-1*: a potential ultrasound contrast agent for tumor imaging. *Pharmaceutics.* 2022;14(6):1198. doi:10.3390/pharmaceutics14061198
14. Feng Y, Hao Y, Wang Y, et al. Ultrasound molecular imaging of bladder cancer using extradomain B fibronectin-targeted biosynthetic GVs. *Int J Nanomed.* 2023;18:4871–4884. doi:10.2147/IJN.S412422
15. Hao Y, Li Z, Luo J, Li L, Yan F. Ultrasound molecular imaging of epithelial mesenchymal transition for evaluating tumor metastatic potential via targeted biosynthetic gas vesicles. *Small.* 2023;19(21):e2207940. doi:10.1002/sml.202207940
16. Yan F, Sun Y, Mao Y, et al. Ultrasound molecular imaging of atherosclerosis for the early diagnosis and therapeutic evaluation of multiple leukocyte-like targeted microbubbles. *Theranostics.* 2018;8(7):1879–1891. doi:10.7150/thno.22070
17. Cui N, Hu M, Khalil RA. Biochemical and biological attributes of matrix metalloproteinases. *Prog mol Biol Transl Sci.* 2017;147:1–73.
18. Xu J, Lu X, Shi GP. Vasa vasorum in atherosclerosis and clinical significance. *Int J mol Sci.* 2015;16(5):11574–11608. doi:10.3390/ijms160511574
19. Chistiakov DA, Melnichenko AA, Myasoedova VA, Grechko AV, Orekhov AN. Role of lipids and intraplaque hypoxia in the formation of neovascularization in atherosclerosis. *Ann Med.* 2017;49(8):661–677. doi:10.1080/07853890.2017.1366041
20. Sedding DG, Boyle EC, Demandt JAF, et al. Vasa vasorum angiogenesis: key player in the initiation and progression of atherosclerosis and potential target for the treatment of cardiovascular disease. *Front Immunol.* 2018;9:706. doi:10.3389/fimmu.2018.00706
21. Li X, Zhang R, Li Z, et al. Quantification of adventitial Vasa vasorum by contrast-enhanced ultrasound imaging in a rabbit model of varying degrees of atherosclerosis. *Sci Rep.* 2017;7(1):7032. doi:10.1038/s41598-017-06127-w
22. Moreno PR, Purushothaman KR, Zias E, Sanz J, Fuster V. Neovascularisation in human atherosclerosis. *Curr mol Med.* 2006;6(5):457–477. doi:10.2174/156652406778018635
23. Kong P, Cui ZY, Huang XF, Zhang DD, Guo RJ, Han M. Inflammation and atherosclerosis: signaling pathways and therapeutic intervention. *Signal Transduct Target Ther.* 2022;7(1):131. doi:10.1038/s41392-022-00955-7
24. Weber C, Noels H. Atherosclerosis: current pathogenesis and therapeutic options. *Nat Med.* 2011;17(11):1410–1422. doi:10.1038/nm.2538
25. Döring Y, Pawig L, Weber C, et al. CXCL12/CXCR4 chemokine ligand/receptor axis in cardiovascular disease. *Front Physiol.* 2014;5:212. doi:10.3389/fphys.2014.00212
26. Döring Y, Noels H, van der Vorst EPC, et al. Vascular CXCR4 limits atherosclerosis by maintaining arterial integrity, as demonstrated in mouse and human studies. *Circulation.* 2017;136(4):388–403. doi:10.1161/CIRCULATIONAHA.117.027646
27. Weiberg D, Thackeray JT, Daum G, et al. Clinical molecular imaging of chemokine receptor CXCR4 expression in Atherosclerotic Plaque Using 68Ga-Pentixafor PET: correlation with cardiovascular risk factors and calcified plaque burden. *J Nucl Med.* 2018;59(2):266–272. doi:10.2967/jnumed.117.196485
28. Buck AK, Stolzenburg A, Hänseid H, et al. Chemokine receptor-directed imaging and therapy. *Methods.* 2017;130:63–71. doi:10.1016/j.ymeth.2017.09.002
29. Kircher M, Herhaus P, Schottelius M, et al. CXCR4-directed theranostics in oncology and inflammation. *Ann Nucl Med.* 2018;32(8):503–511. doi:10.1007/s12149-018-1290-8
30. Dweck MR, Aikawa E, Newby DE, et al. Non-invasive molecular imaging of disease activity in atherosclerosis. *Circ Res.* 2016;119(2):330–340. doi:10.1161/CIRCRESAHA.116.307971
31. Piraner DI, Farhadi A, Davis HC, et al. Going deeper: biomolecular tools for acoustic and magnetic imaging and control of cellular functions. *Biochemistry.* 2017;56(39):5202–5209. doi:10.1021/acs.biochem.7b00443
32. D'souza AA, Shegokar R. Polyethylene glycol (PEG): a versatile polymer for pharmaceutical applications. *Expert Opin Drug Deliv.* 2016;13(9):1257–1275. doi:10.1080/17425247.2016.1182485
33. Virmani R, Kolodgie FD, Burke AP, et al. Atherosclerotic plaque progression and vulnerability to rupture: angiogenesis as a source of intraplaque hemorrhage. *Arterioscler Thromb Vasc Biol.* 2005;25(10):2054–2061. doi:10.1161/01.ATV.0000178991.71605.18
34. Sever PS, Dahlöf B, Poulter NR, et al. Prevention of coronary and stroke events with atorvastatin in hypertensive patients with average or lower-than-average cholesterol concentrations in the Anglo-Scandinavian Cardiac Outcomes Trial--Lipid Lowering Arm (ASCOT-LLA): a multicenter randomized controlled trial. *Drugs.* 2004;64(Suppl 2):43–60. doi:10.2165/00003495-200464002-00005
35. Kim Y, Lobatto ME, Kawahara T, et al. Probing nanoparticle translocation across the permeable endothelium in experimental atherosclerosis. *Proc Natl Acad Sci U S A.* 2014;111(3):1078–1083. doi:10.1073/pnas.1322725111
36. Tapia-Vieyra JV, Delgado-Coeollo B, Mas-Oliva J. Atherosclerosis and cancer; a resemblance with far-reaching implications. *Arch Med Res.* 2017;48(1):12–26. doi:10.1016/j.arcmed.2017.03.005
37. Shi Y, van der Meel R, Chen X, Lammers T. EPR effect and beyond: strategies to improve tumor targeting and cancer nanomedicine treatment efficacy. *Theranostics.* 2020;10(17):7921–7924. doi:10.7150/thno.49577

38. Lobatto ME, Calcagno C, Millon A, et al. Atherosclerotic plaque-targeting mechanism of long-circulating nanoparticles established by multimodal imaging. *ACS Nano*. 2015;9(2):1837–1847. doi:10.1021/nn506750r
39. Shinde VR, Revi N, Murugappan S, Singh SP, Rengan AK. Enhanced permeability and retention effect: a key facilitator of solid tumor targeting by nanoparticles. *Photodiagnosis Photodyn Ther*. 2022;39:102915. doi:10.1016/j.pdpdt.2022.102915
40. Sheng X, Ding S, Ge H, et al. Intracoronary infusion of alprostadil and nitroglycerin with targeted perfusion microcatheter in STEMI patients with coronary slow flow phenomenon. *Int J Cardiol*. 2018;265:6–11. doi:10.1016/j.ijcard.2018.04.119
41. Shakya G, Cattaneo M, Guerriero G, Prasanna A, Fiorini S, Supponen O. Ultrasound-responsive microbubbles and nanodroplets: a pathway to targeted drug delivery. *Adv Drug Deliv Rev*. 2024;206:115178. doi:10.1016/j.addr.2023.115178

International Journal of Nanomedicine

Publish your work in this journal

The International Journal of Nanomedicine is an international, peer-reviewed journal focusing on the application of nanotechnology in diagnostics, therapeutics, and drug delivery systems throughout the biomedical field. This journal is indexed on PubMed Central, MedLine, CAS, SciSearch®, Current Contents®/Clinical Medicine, Journal Citation Reports/Science Edition, EMBase, Scopus and the Elsevier Bibliographic databases. The manuscript management system is completely online and includes a very quick and fair peer-review system, which is all easy to use. Visit <http://www.dovepress.com/testimonials.php> to read real quotes from published authors.

Submit your manuscript here: <https://www.dovepress.com/international-journal-of-nanomedicine-journal>

Dovepress
Taylor & Francis Group